Aalborg Universitet

AALBORG UNIVERSITY
DENMARK

Integrated Millimeter-Wave Wideband End-Fire 5G Beam Steerable Array and Low-Frequency 4G LTE Antenna in Mobile Terminals

Taheri, Mohammad Mehdi Samadi; Abdipour, Abdolali; Zhang, Shuai; Pedersen, Gert F.

Integrated Millimeter-Wave Wideband End-Fire 5G Beam Steerable Array and Low-Frequency 4G LTE Antenna in Mobile Terminals

Mohammad Mehdi Samadi Taheri, *Student Member, IEEE*, Abdolali Abdipour, *Senior Member, IEEE*, Shuai Zhang, *Senior Member, IEEE*, and Gert Frølund Pedersen, *Senior Member, IEEE*

Abstract— **In this paper, a novel technique of collocating millimeter-wave end-fire 5G beam steerable array antenna with a low-frequency PIFA is presented. In this technique, the low-frequency antenna can be transparent by using some grating strips between the low- and high-frequency antennas. A quad-element mm-wave array with end-fire radiation patterns operating in 22-31 GHz is integrated with a dual-band low-frequency PIFA in a mobile terminal. The novelty of this paper is the collocation of high-frequency end-fire 5G antenna array with an old generation low-frequency antenna such as 4G in small space in the mobile terminal without interfering with the radiation pattern and impedance matching of both low- and high-frequency antennas. The proposed 5G antenna covers the 22-31 GHz and can scan ± 50 degree with the scan loss of better than 3 dB. The coverage efficiency of the proposed mm-wave 5G antenna is better than 50 and 80 % for a minimum gain of 4 and 0 dBi in 22-31 GHz, respectively. The gain of the high-frequency antenna array is better than 9.5 dBi at 28 GHz. The low-frequency antenna covers some practical 4G LTE bands from 740-960 MHz and 1.7-2.2 GHz bands. The measured results in both low- and high-frequency agree well with the simulations.**

Index Terms—**Antenna, Millimeter-wave, Handset antennas, 5G, Collocation of 5G and 4G antenna, 4G, Phased array antenna.**

I. INTRODUCTION

WITH rapid demand on extremely high data rates communication, researchers have been urged towards millimeter-wave (mm-wave) technology [1]. There are several challenges in mm-wave propagations in a mobile terminal including path loss, transmission loss, shadowing and user effects [2]. Thus, high gain antennas with steerable beams are

Mohammad Mehdi Samadi Taheri, and Abdolali Abdipour are with Microwave/millimeter-wave and Wireless Communications Research Laboratory, Electrical Engineering Department, Amirkabir University of technology (Tehran polytechnic), Tehran, Iran (email: mehdisamadi@aut.ac.ir, abdipour@aut.ac.ir). (Corresponding author: Abdolali Abdipour).

Shuai Zhang, and Gert Frølund Pedersen are with the Department of Electronic Systems, Aalborg University, Denmark (email: sz@es.aau.dk, gfp@es.aau.dk)

desirable for mm-wave 5G applications [3]. Different frequency spectrums have been proposed for the 5G scenarios. Due to the smallest attenuation absorption, the 28 GHz frequency is one of the best choices for the 5G frequency range [1].

Several mm-wave antennas have been proposed for the 5G scenarios [4-6]. However, in the literature few works have been reported for the mm-wave 5G antenna in the mobile handsets [7-11]. In [7], an overview of four design consideration is presented in which criteria for the mm-wave 5G cellular handset phased array antennas at 60 GHz is reported. In [8], by using slots on a handset chassis in different positions 3D beam coverage can be attained with the help of exciting surface currents at 28 GHz. Three different oriented arrays have been used to cover 3D beam coverage [9]. However, the fabricated prototype has not been presented and implementation of this topology is a challenging issue. Statistical studies of user effects on a mobile terminal antenna at 28 GHz have been investigated [10]. In [11], a new concept of coverage efficiency has been introduced that is related to antenna efficiency, antenna gain, beam scanning and coverage area of the antenna. The coverage efficiency is an important factor for 5G mobile terminal antennas and is defined in the formula (1) in [11].

In current mobile handsets, there are very small space (small clearance) left after placing phone components and low-frequency 2G/3G/4G antennas such as the ones in [12-14]. One of the solutions is to integrate mm-wave 5G arrays and the low-frequency antennas together. The integration of mm-wave and low-frequency antennas is a quite challenging and interesting topic nowadays. Furthermore, mm-wave arrays with end-fire radiation patterns are more desired in mobile terminals, which are more immune from user shadowing (in data mode) [12], and the metallic screen effect on array radiation patterns than the ones with broadside radiation patterns. Meanwhile, the integration of an end-fire 5G array and a low-frequency antenna in a small space is more challenging than the broadside one, due to the interference of the low-frequency antenna on the 5G array. The integrated 4G antennas and a mm-wave 5G array is reported in [15]. However, this high-frequency antenna array has some drawbacks such as limited bandwidth, broadside radiation patterns, and fixed radiation pattern beams instead of beam steering. The complexity of the multi-layer fabrication is another challenging issue in [15].

In this paper, a novel concept of the anti-reflective layer technique with grating strips is proposed. In this technique, end-fire mm-wave 5G beam steering array antenna is collocated with the planar low-frequency antenna in the mobile terminal in a small space with minimum interference.

II. ANTI-REFLECTIVE LAYER WITH GRATING STRIPS

A. Introduction of the anti-reflective technique with grating strips

There is a small space (small clearance) on the top or bottom of a mobile handset for placing low- and high-frequency antennas together. In the collocation of low- and high-frequency antennas two methodologies can be applied in a mobile terminal:

a) Placing the 5G mm-wave antenna array in front of the low-frequency planar antenna.

b) Placing the 5G mm-wave antenna array in the behind of the low-frequency planar antenna.

In the case (a), placement of the low-frequency antenna behind the high-frequency antenna in a small clearance (small L_c, as shown in Fig. 4) has some drawbacks. First of all, due to the small clearance, if the space between the low-frequency antenna and the ground plane is reduced the low-frequency antenna efficiency and impedance bandwidth degrade and the antenna cannot operate in such a wide band at low frequencies. Secondly, when the high-frequency antennas replaced in front of the low-frequency antenna in the same top or bottom plane, the feeding network of the high-frequency antennas is difficult to realize since it has to cross the low-frequency antenna. If these low and high-frequency antennas are placed in different planes (one on the top and the other on the bottom) strong mutual coupling between them degrade the antenna performance totally. So, it degrades the low- and high-frequency operation in terms of impedance matching and radiation patterns.

In the case (b), the low-frequency antenna blocks the radiation patterns of the end-fire mm-wave array if placed in front of the array. Consequently, the wave cannot propagate in the main direction. So, it is extremely challenging to collocate these low- and high-frequency end-fire antennas in a small space without degrading their performance. In the following, the authors propose a novel technique to solve this problem.

In this technique, the low-frequency antenna can be transparent by using some grating strips between the low- and high-frequency antennas which are configured in case (b). The mechanism of this transparency is based on the anti-reflective layer technique. In this method, some grating strips are utilized between the low- and high-frequency antennas. By adjusting the grating strip parameters, the wave at high frequencies can propagate in the end-fire direction through the low-frequency antenna with minimum interference.

B. Simple model study

In this section, the effect of using grating strips as an anti-reflective layer between the low- and high-frequency antennas is studied. The prototype of the antenna is shown in Fig. 1. The low-frequency antenna is a simple planar inverted-F antenna (PIFA) and the high-frequency antennas can be any type of end-fire radiation pattern antennas. For simplicity, a quad-element array of the folded dipoles has been used in this study. As seen in Fig. 1, some grating strips are placed between the low- and high-frequency antennas. In this arrangement, when a wave at mm-wave frequency range propagates from the high-frequency antenna elements, the grating strips act as an anti-reflective layer such that one portion of the wave is transmitted and another portion is reflected back (e.g., towards the high-frequency antenna elements). The transmitted portion of the wave can further be diffracted at the low-frequency antenna, with some of the waves being transmitted and some being reflected by the low-frequency antenna. As shown in Fig. 1, the two parts of reflected waves (i.e., first portion reflected by the grating strips, shown by dashed blue lines, and second portion reflected by the low-frequency antenna, shown by solid red lines) reach the high-frequency antenna elements. In order to cancel these two reflected waves at high-frequency antennas, the two reflected waves must be out of phase. That means the path that waves go through the grating strips to the low-frequency antenna and reflect back should be an odd number of half wavelength. This phenomenon is represented by (1).

$$2 \times (L_2 + L_1) - 2 \times L_2 = 2L_1$$
$$2L_1 = (2n+1)\lambda/2 \tag{1}$$

Therefore, L_1 should be approximately a quarter of the wavelength. Due to spacing L_1, the two reflected waves are out of phase so they cancel each other when they reach to the high-frequency antennas. In this way, the wave from high-frequency can propagate in the end-fire direction without interference.

As a proof of concept three scenarios have been modeled to verify the effect of anti-reflective grating strips:

1- Only high-frequency antennas exist in the mobile terminal.
2- Collocated low- and high-frequency antennas without grating strips in the mobile terminal.
3- Collocated low- and high-frequency antennas with grating strips in the mobile terminal.

The 3D realized gain radiation patterns of the end-fire mm-wave antenna in the above three scenarios at 28 GHz are studied and shown in Fig. 2. When the low- and high-frequency antennas are collocated without grating strips, the wave reflected downward and the radiation pattern is not totally end-fire, as shown in Fig. 2(b). By inserting the grating strips between the low- and high-frequency antennas, the end-fire radiation pattern can be obtained as shown in Fig. 2(c). The results show that the collocated low- and high-frequency antennas with grating strips have the similar results as the scenario number 1 in which only high-frequency antennas exist. The distance between the grating strips and the low-frequency antenna (L_1) plays the most important role in the effectiveness of the grating anti-reflective layer. The other parameters, such as the strips length (L_s), and the spacing between the strips (S)
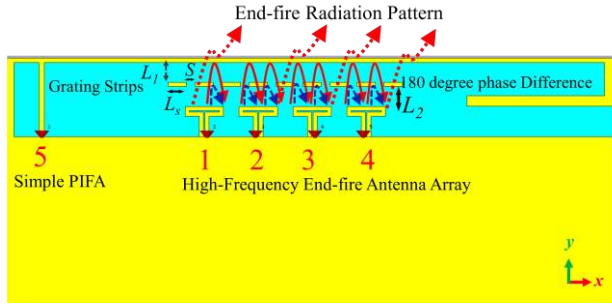
Fig. 1. The integrated low-frequency PIFA and mm-wave end-fire antenna array with the concept of anti-reflective grating strips.
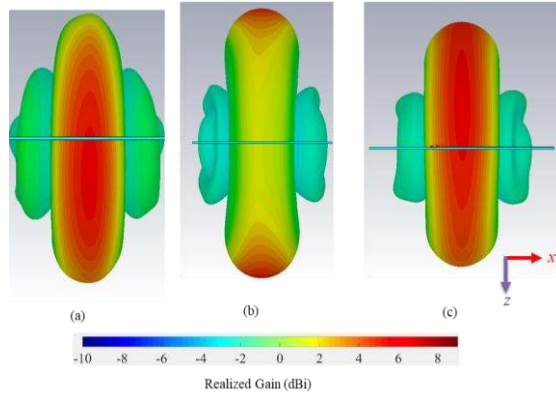

Fig. 2. The 3D realized gain radiation patterns (dBi) of end-fire mm-wave antenna array in different scenario at 28 GHz: (a) only the mm-wave array without anti-reflective grating strips and the low-frequency antenna, (b) collocated low- and high-frequency antennas without anti-reflective grating strips, and (c) the collocated antennas with anti-reflective grating strips.

affect the radiation pattern, the level of realized gain, and impedance matching. In this configuration, the final optimized dimensions of these three parameters are as follows:
L_s = 1.8 mm, S = 0.85 mm, and L_1 = 2 mm.
Although the bandwidth of the high-frequency antenna is wide (22-31 GHz), the fractional bandwidth, due to the high-frequency operation, is limited to around 30%. So in Fig. 1, two portions of the reflected waves reach to the high-frequency antenna with phase difference of 150º-200º in whole operating bandwidth. Therefore, in the proposed narrow fractional bandwidth the phase deviation from 180º is less than 30º within the bandwidth. One can suppose that the phase can be canceled in upper and lower band of operation. As shown in Fig. 1, the two parts of reflected waves (from the low-frequency antenna and the grating strips) cancel each other on the high-frequency antenna. Therefore, the reflected waves have very limited effect on the radiation pattern and resonance of the high-frequency antennas. The reflection coefficient of antenna number three in the three scenarios have been shown in Fig. 3. The results show that S_{33} in the case of collocated antennas with grating strips is almost the same as topology in which only high-frequency antennas exist. The S_{33} in the case of collocated antennas without grating strips is also presented in Fig. 3 as a
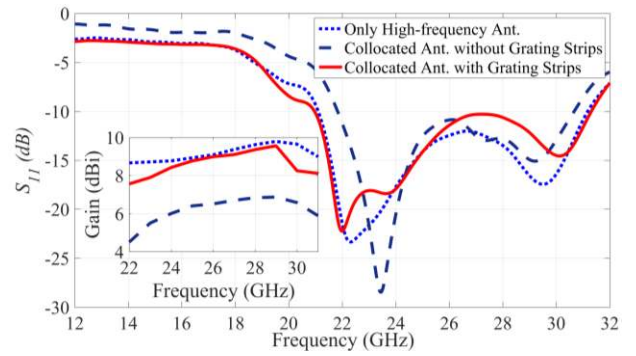

Fig. 3. The reflection coefficient of antenna three in collocated topology at three different scenarios, and the total realized gain (dBi) of end-fire mm-wave high-frequency antenna array in collocated low and high-frequency antenna in different scenarios in broadband frequency range in the inner plot.

comparison, where a narrower bandwidth is observed due to the reflected waves from the low-frequency antenna. In addition, the effect of adding grating strips in the collocated topology on antenna gain in three different scenarios have been illustrated in Fig. 3 in inner plot. It is obvious when there are no grating strips in the collocated topology the beam has squint and the pattern is not totally end-fire. So the antenna gain in the end-fire direction decreases in comparison with the situation that only high-frequency antennas exist. From Fig. 3, one can see that the antenna gains and radiation pattern in scenarios number 1 and number 3 are almost the same where the difference in antenna gain is less than 1 dB in the broad band frequency. This means the anti-reflective grating strips solve the blockage problem of the low-frequency antenna in the collocated topology.

III. ANTENNA DESIGN

In this section, the anti-reflective layer method is used to collocate 5G mm-wave end-fire antenna array with low-frequency dual-band PIFA. The configurations of the proposed collocated low- and high-frequency antennas are shown in Fig. 4. The antennas are printed on a high-frequency low loss Nelco N9000 substrate with a relative permittivity of 2.2, loss tangent of 0.0009 and thickness of 0.764 mm. The total dimensions of the antenna are 70×120×0.764 mm^3 which is the standard dimension for a mobile handset. The antenna dimensions after optimization are as follows:
L_1 = 2 mm, L_2 = 3.85 mm, L_3 = 3.05 mm, L_4 = 0.75 mm, L_5 = 2 mm, L_6 = 5 mm, L_7 = 2.8 mm, L_8 = 23.7 mm, L_9 = 5.2 mm, L_{10} = 7 mm, L_{11} = 3.8 mm, L_{12} = 14.5 mm, L_{13} = 19 mm, L_{14} = 27 mm, L_d = 2.8 mm, L_r = 5.05 mm, L_c = 9 mm, W = 0.4 mm, S = 0.15 mm, g = 0.2 mm, g_1 = 1 mm, S_r = 0.25 mm, S_d = 2.5 mm, W_r = 0.4 mm, W_d = 0.4 mm, W_L = 0.4 mm, W_1 = 1 mm, D_r = 3.6 mm, D_d = 2 mm, X_s = 1.45 mm, X_{sp} = 5.3 mm, X_{sub} = 70 mm, Y_{sub} = 120 mm, and H_{sub} = 0.764 mm. H_{sub} is the thickness of substrate.

The high-frequency antenna is a mm-wave array with quad-element folded dipole. The inter-element spacing (X_{sp}) is half-wavelength at 28 GHz. To improve the impedance matching of the high-frequency array elements, four strip reflectors are added on the back copper layer of the PCB. These
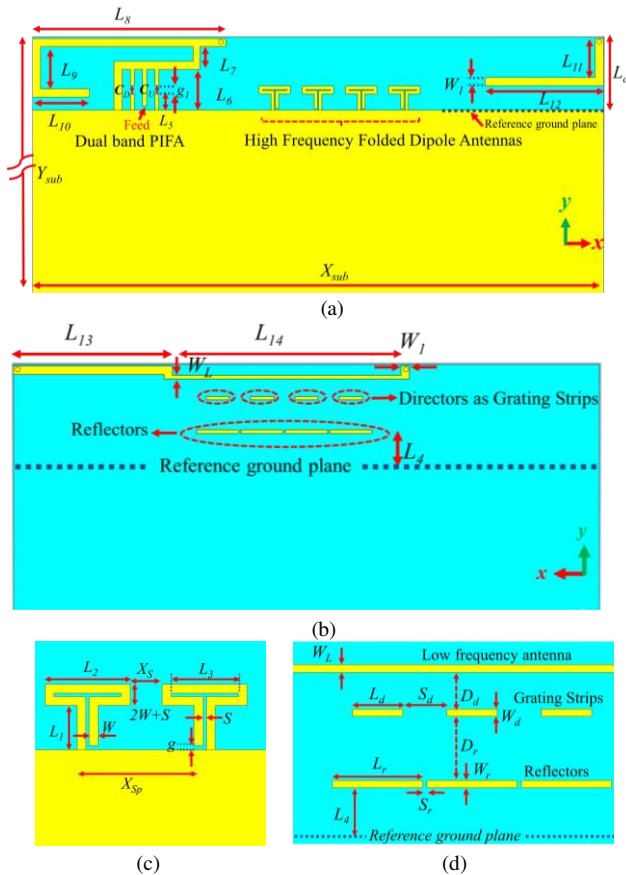
Fig. 4. Proposed collocated 5G mm-wave antenna array with dual-band low-frequency PIFA. (a) top view, (b) bottom view, (c) top view of the high-frequency antenna with more details and enlargement, and (d) bottom view of high-frequency antenna with more details and enlargement.

part of the short edge can be left for other components of the mobile handset such as USB, speaker, camera and so on. A small gap (g), as shown in Fig. 4 (c), is added to feed the high-frequency antenna. In order to increase the total scan angle and coverage efficiency in presence of large ground plane in collocated configuration, the high-frequency antennas have been arranged alternatively. It means the first antenna has been fed from right side and the second one fed from the left side and so on. This feeding configuration needs 180º phase difference for the neighboring elements.

The low-frequency antenna is a dual wideband PIFA. The dual wideband property is realized by adding two loop tuning branches at the feeding point of the PIFA as referred in [14]. By tuning the capacitance C_D and C_U, wide band performance in dual frequency bands from 740-960 MHz and 1.7-2.2 GHz has been achieved. The value of capacitance after optimization has been chosen C_D = 5.6 pF and C_U = 1.2 pF.

IV. SIMULATION AND MEASUREMENT RESULTS

The integrated mm-wave quad-element antenna array with the dual-band low-frequency antenna system has been modeled and simulated with CST microwave studio software. The optimized prototype with feeding cables has been fabricated as shown in Fig. 5 (a-b), and also measured as illustrated in Fig. 5 (c-f). Low-loss cables (working from low frequencies to mm-wave) have been used for the feeding structure of the high-frequency antennas in the prototype. As aforementioned, the neighboring elements of the mm-wave array have 180º phase difference. This is achieved by accurately measuring of the phase of the cable by PNA and cutting them in a precise manner to achieve accurate 180º phase difference at 28 GHz. Whereas the length of cables for antenna 2 and 4 is a bit longer than the cables for antenna number 1 and 3 to create 180º phase difference. In the simulations, the feeding cables haven been modeled and their effects have been included.

The S-parameters of the fabricated low- and high-frequency antennas have been measured with a 67 GHz four port N5227A Keysight PNA as illustrated in Fig. 5 (c). The measured S-parameters (reflection coefficients and mutual coupling) of the proposed high-frequency antenna elements are shown in Fig. 6. In both simulations and measurements, the -10 dB bandwidth is around 22-31 GHz. The simulation isolation is over 15 dB and the measured one is over 13 dB within the whole band (see Fig. 6). The low-frequency antenna in the proposed collocated topology has a good reflection coefficient of better than -6 dB in both simulation and measurement, from 740-960 MHz and 1.7-2.2 GHz that covers some practical 4G LTE bands. The mutual coupling between array elements (port 1-4) and low-frequency PIFA (port 5) has been measured from DC- 34 GHz, where the mutual coupling is less than -40 dB at all frequencies (see Fig. 6). In general, the simulated and measured S-parameters are very similar.

The radiation patterns of the fabricated low- and high-frequency antennas have been measured in an anechoic chamber, as shown in Fig. 5 (d-e). The 3D radiation patterns of the high-frequency antenna elements are measured in a large anechoic chamber one

reflectors can also improve the antenna performance (such as gain and front to back ratio), and reduce the large ground effect on antenna radiation patterns. It has been studied that the placement of the grating strips on the front or back side of copper layer in the PCB has the similar effects on the end-fire radiation patterns. Placing the grating strips on the back layer can compensates the large ground plane effect on the mm-wave radiation patterns and makes the patterns more symmetric. Furthermore, When the low-frequency antenna placed in the same copper layer of the grating strips, the impedance bandwidth of the high-frequency antenna gets better. So as shown in Fig. 4 (b), part of the low-frequency antenna is placed on the same PBC copper layer of the grating strips. As stated in Section II, the distance between the grating strips and the low-frequency antenna is the most important parameter for the anti-reflective layer technique. So in a special case, as shown in Fig. 4 (b), the grating strips can be further interpreted as a director for each high-frequency folded dipole and with the same distance away from the low-frequency antenna. In this way, the gain of the high-frequency antenna can also be improved besides realizing end-fire radiation. In addition, the high-frequency array is placed at the central part of the handset short edge, which is only for proof of concept. In practice, it can also be placed close to the corner of the short edge without changing the end-fire radiation property. In this way, the central
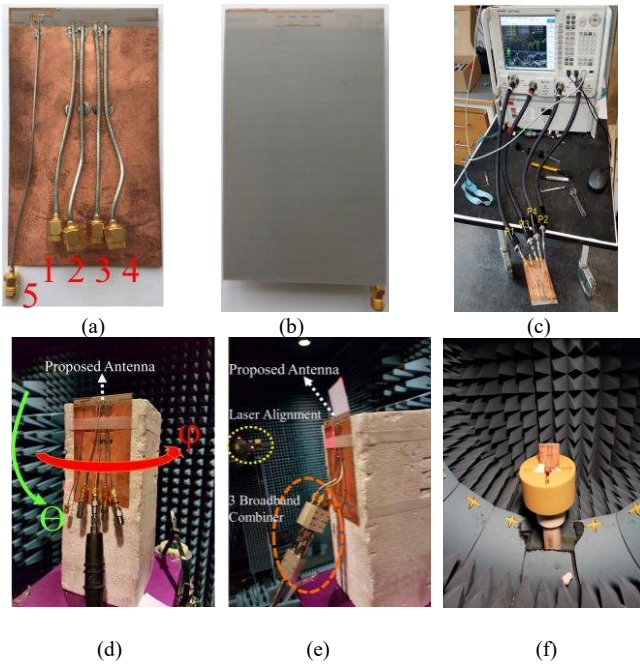
Fig. 5. The prototype of the proposed integrated fabricated antennas: (a) top view, and (b) bottom view. (c) S-parameter measurement with PNA. (d) Measurement of each mm-wave element in collocated topology in a large chamber. (e) Measurement of a mm-wave array of quad-elements with the combiners in collocated topology. (f) Measurement of low-frequency antenna at SATIMO chamber.
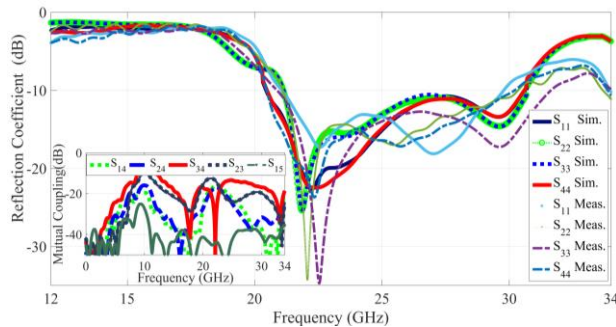

Fig. 6. The S-parameters (simulated and measured reflection coefficients and measured isolation) of the fabricated collocated mm-wave antenna elements.

Fig. 7. The simulated and measured normalized radiation pattern (dB) of the high-frequency antenna array in the H-plane (x-y plane) at different frequencies: (a-c) Each element radiation pattern; (d-f) radiation patterns of the array with the wideband combiners. (g-i) The combination of the measured radiation patterns (dB) of all array elements with different phase shift.

by one as shown in Fig. 5 (d). The phase center of each element is aligned precisely with laser alignment as shown in Fig. 5 (e). As shown in Fig. 5 (d), a positioner rotates in ϕ direction of 0°-360° with the step of 2 degrees, while a scan arm scans in θ direction of 0°- 140° with the step of 2 degrees. A dual polarized probe horn antenna for two orthogonal polarization measurement is attached at the end of the scan arm. The antenna under test is oriented in such a way that the back of the antenna is placed at θ = 180º. The measured and simulated radiation patterns of the first and second end-fire high-frequency array elements in the H-plane (x-y plane) at 22, 26, and 30 GHz are provided in Fig. 7 (a-c), respectively. After measuring each element radiation pattern, the total radiation pattern of the quad-element array in phase has been measured with a combination of three 3-dB broadband Pasternack combiners up to 40 GHz. The connection of the combiners has been shown in Fig. 5 (e). The simulated and measured radiation pattern of the
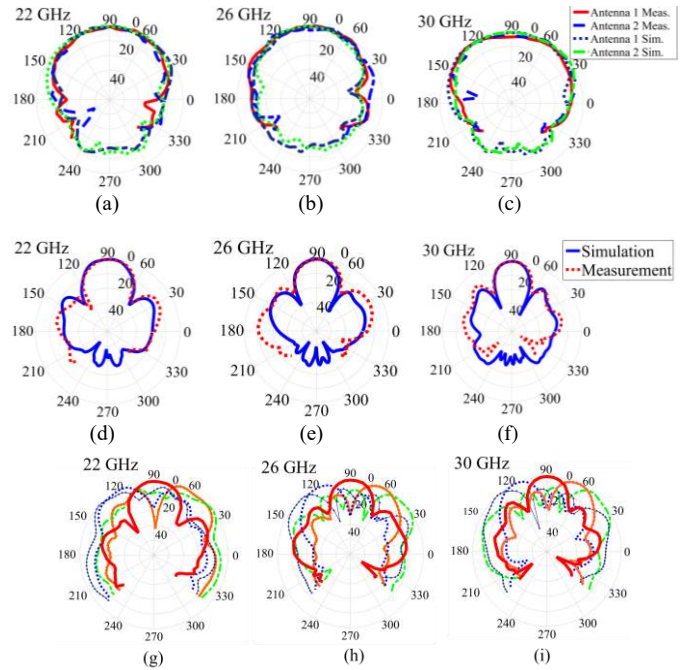
proposed array with combiners at 22, 26, and 30 GHz in H-plane (x-y plane) is shown in Fig. 7 (d-f), respectively. It is noticed that the main beam of the radiation pattern and the half power beamwidth in both simulations and measurements agree well. The radiation pattern measurement is also carried out with the 67 GHz four-port PNA, which measured the amplitude and phase of the radiation pattern for each array element from 22-31 GHz. The combination of the measured radiation pattern of collocated array with different phase shifts at 22, 26, and 30 GHz is shown in Fig. 7 (g-i), respectively. The proposed high-frequency antenna array has a wide scan angle of ±50 degrees in H- plane (*x-y* plane) with scan loss better than 3 dB. In this paper, the array element is fed with ideal amplitudes and phase for beam steering.

The realized gain of the collocated high-frequency antenna array at different frequencies has been measured and shown in Fig. 8. The simulated and measured gain of the second element is also shown in the same figure. It is seen that the array has the measured gain of more than 8 dBi in 25-30.5 GHz. The measured antenna array gain around 28 GHz is more than 9.5 dBi, which can be suitable for 5G applications. The beam steering capability of the mm-wave array in collocated low- and high-frequency antenna topology in different three scenarios has been investigated in broadband. The antenna peak gain at 30-degree scanning angle at three scenarios are given in Fig. 8. Results show in the collocated topology with grating strips the antenna gain and beam steering capability are almost the same as the scenario where only high-frequency antenna array exists. The scan loss is better than 1.8 dB in the whole operating bandwidth in scan angle of 30-degree in the collocated array
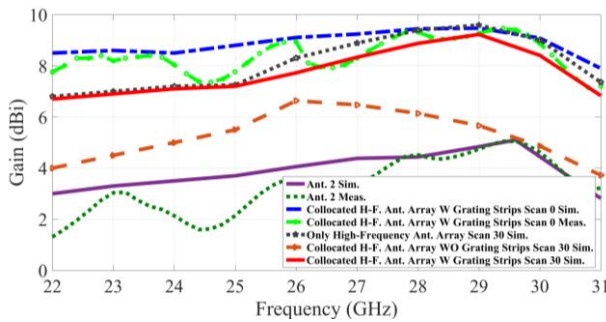
Fig. 8. The simulated and measured gain of the second array element, and the gain of the high-frequency array in different scenarios and scan angles.
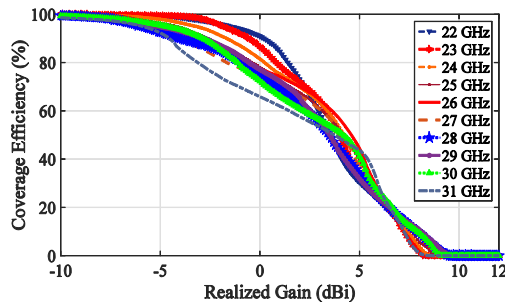

Fig. 9. The coverage efficiency of the proposed end-fire mm-wave array in the collocated topology at different frequencies.

with grating strips. In the collocated antenna without grating strips, the radiation pattern is not totally end-fire and the gain also degrades quite much when the beam steered. The total efficiency and realized gain of the low-frequency antenna has been tested in Satimo, as illustrated in Fig. 5 (f). The measured total efficiency is better than 64% and 65% in the bands of 740-960 MHz and 1.7-2.2 GHz, respectively. Also the measured gain is more than 0.35 dBi and 3.6 dBi in 740-960 MHz band and 1.7-2.2 GHz band, respectively.

In order to quantify the beam coverage performance, the coverage efficiency is calculated by the formula (1) in [13]. The coverage efficiency gives an intuitive feeling about how large solid angle can be covered by beam steerable array antennas in a user equipment. The coverage efficiency of the proposed collocated high-frequency antenna array is shown in Fig. 9. One can see that the proposed array can cover 80 percent of spheres with minimum gain of 0 dBi and 50 percent of the sphere with a minimum gain of 4 dBi at 22-31 GHz which is a quite large coverage for a quad-element antenna array.

V. CONCLUSION

A novel concept of the anti-reflective layer with grating strips has been proposed for collocating an end-fire mm-wave 5G array and a low-frequency antenna in mobile terminals. By applying the grating strips technique, the proposed collocated high-frequency antenna array operates with minimum interference with the low-frequency antenna in terms of radiation pattern and impedance matching. The mm-wave high-frequency antenna operates from 22-31 GHz both in impedance matching and the end-fire radiation pattern that covers multi band for 5G applications such as 24 and 28 GHz. The array can scan ±50 degrees with end-fire radiation, which leads to a good coverage efficiency. The total scan pattern and

coverage efficiency of the proposed high-frequency array proves that the antenna can cover 50 and 80 percent of the sphere with a minimum gain of 4 dBi and 0 dBi at 22-3 GHz, respectively. The low-frequency antenna has also been measured that can cover dual-band of 740-960 MHz and 1.7-2.2 GHz with good total efficiency and realized gain.

REFERENCES

[1] T. S. Rappaport, S. Sun, R. Mayzus, H. Zhao, Y. Azar, K. Wang, G. N. Wong, J. K. Schulz, M. Samimi, and F. Gutierrez, "Millimeter wave mobile communications for 5G cellular: it will work!," *IEEE Access*, vol. 1, pp. 335-349, 2013.
[2] K. Zhao, J. Helander, D. Sjöberg, S. He, T. Bolin and Z. Ying, "User body effect on phased array in user equipment for the 5G mmwave communication system," *IEEE Antennas Wireless Propag. Lett.,* vol. 16, pp. 864-867, 2017.
[3] T. S. Rappaport, F. Gutierrez, E. Ben-Dor, J. N. Murdock, Y. Qiao and J. I. Tamir, "Broadband millimeter-wave propagation measurements and models using adaptive-beam antennas for outdoor urban cellular communications," *IEEE Trans. Antennas Propag.*, vol. 61, no. 4, pp. 1850-1859, April 2013.
[4] O. M. Haraz, A. Elboushi, S. A. Alshebeili and A. R. Sebak, "Dense dielectric patch array antenna with improved radiation characteristics using EBG ground structure and dielectric superstrate for future 5G cellular networks," *IEEE Access*, vol. 2, pp. 909-913, 2014.
[5] H. Chu and Y. X. Guo, "A filtering dual-polarized antenna subarray targeting for base stations in millimeter-wave 5G wireless communications," *IEEE Trans. Compon. Packag. Manufact. Technol*, vol. 7, no. 6, pp. 964-973, June 2017.
[6] H. Aliakbari, A. Abdipour, A. Costanzo, D. Masotti, R. Mirzavand and P. Mousavi, "ANN-based design of a versatile millimetre-wave slotted patch multi-antenna configuration for 5G scenarios," *IET Microw. Antennas Propag.*, vol. 11, no. 9, pp. 1288-1295, June 2017.
[7] W. Hong, K. h. Baek and S. Ko, "Millimeter-wave 5G antennas for smartphones: overview and experimental demonstration," *IEEE Trans. Antennas Propag.*, vol. 65, no. 12, pp. 6250-6261, Dec. 2017.
[8] S. Zhang, X. Chen, I. Syrytsin and G. F. Pedersen, "A planar switchable 3D-coverage phased array antenna and its user effects for 28 GHz mobile terminal applications," *IEEE Trans. Antennas Propag.*, vol. 65, no. 12, pp. 6413-6421, Dec. 2017.
[9] N. Ojaroudiparchin, M. Shen, S. Zhang and G. F. Pedersen, "A switchable 3-D-coverage-phased array antenna package for 5G mobile terminals," *IEEE Antennas Wireless Propag. Lett.*, vol. 15, pp. 1747-1750, 2016.
[10] I. Syrytsin, S. Zhang, G. Pedersen, K. Zhao, T. Bolin and Z. Ying, "statistical investigation of the user effects on mobile terminal antennas for 5G applications," *IEEE Trans. Antennas Propag.*, vol. 65, no. 12, pp. 6596-6605, Dec. 2017.
[11] J. Helander, K. Zhao, Z. Ying and D. Sjöberg, "Performance analysis of millimeter-wave phased array antennas in cellular handsets," *IEEE Antennas Wireless Propag. Lett.*, vol. 15, pp. 504-507, 2016.
[12] I. Syrytsin, S. Zhang and G. F. Pedersen, "performance investigation of a mobile terminal phased array with user effects at 3.5 GHz for LTE advanced," *IEEE Antennas Wireless Propag. Lett.*, vol. 16, pp. 1847-1850, 2017.
[13] C. Deng, Y. Li, Z. Zhang and Z. Feng, "Planar printed multi-resonant antenna for octa-band WWAN/LTE mobile handset," *IEEE Antennas Wireless Propag. Lett.*, vol. 14, pp. 1734-1737, 2015.
[14] S. Jeon, S. Oh, H. H. Kim and H. Kim, "Mobile handset antenna with double planar inverted-E (PIE) feed structure," *Electron. Lett.*, vol. 48, no. 11, pp. 612-614, May 2012.
[15] R. Hussain, A. T. Alreshaid, S. K. Podilchak and M. S. Sharawi, "Compact 4G MIMO antenna integrated with a 5G array for current and future mobile handsets," *IET Microw. Antennas Propag.*, vol. 11, no. 2, pp. 271-279, Jan. 2017.